Materials Research Letters

ISSN: 2166-3831 (Online) Journal homepage: www.tandfonline.com/journals/tmrl20

Making glassy solids ductile at room temperature by imparting flexibility into their amorphous structure

Zhao Fan, Jun Ding & Evan Ma

To cite this article: Zhao Fan, Jun Ding & Evan Ma (2018) Making glassy solids ductile at room temperature by imparting flexibility into their amorphous structure, Materials Research Letters, 6:10, 570-583, DOI: 10.1080/21663831.2018.1503198

To link to this article: https://doi.org/10.1080/21663831.2018.1503198

© 2018 The Author(s). Published by Informa UK Limited, trading as Taylor & Francis Group

View supplementary material

Published online: 08 Aug 2018.

Submit your article to this journal

Article views: 4483

View related articles

View Crossmark data

Citing articles: 6 View citing articles

Full Terms & Conditions of access and use can be found at
https://www.tandfonline.com/action/journalInformation?journalCode=tmrl20

MATER. RES. LETT.
2018, VOL. 6, NO. 10, 570–583
https://doi.org/10.1080/21663831.2018.1503198

PERSPECTIVE

OPEN ACCESS

Making glassy solids ductile at room temperature by imparting flexibility into their amorphous structure

Zhao Fan[a], Jun Ding[b] and Evan Ma[a]

[a]Department of Materials Science and Engineering, Johns Hopkins University, Baltimore, MD 21218, USA; [b]Materials Sciences Division, Lawrence Berkeley National Laboratory, Berkeley, 94720, CA, USA

ABSTRACT

Making glasses ductile at room temperature is a daunting challenge, but has been shown to be feasible in recent years. We explain the plastic flow from the standpoint of the flexibility available in the amorphous structure: imparting flexibility into the structure facilitates bond switching needed to mediate shear transformations to carry strain. This structure–property correlation is demonstrated using molecular dynamics simulation data. The flexibility can be improved via ultrafast quench or rejuvenation. In particular, the flexibility volume parameter offers a quantitative metric to explain the flexibility and deformability, even for glasses where the commonly cited free volume is not applicable.

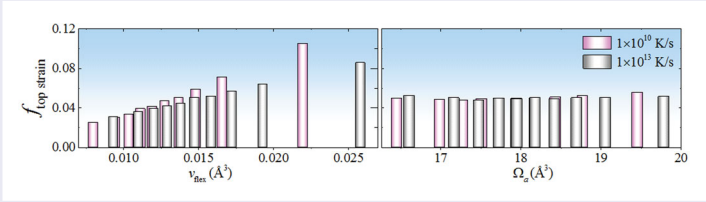

IMPACT STATEMENT

This Perspective demonstrates using examples and models that it is the flexibility rather than the excess volume that can be tuned to facilitate plastic flow and ductility in glassy materials.

ARTICLE HISTORY
Received 2 July 2018

KEYWORDS
Glassy or amorphous materials; plastic flow and ductility; molecular dynamics; structure–property correlation; flexibility versus free volume

1. Introduction

Glassy or amorphous materials are ubiquitous, offering many useful properties in our daily lives [1–7]. But they suffer from one major drawback, being usually brittle at room temperature (RT) [8–13]; their shape change relies upon viscous flow near or above the glass transition temperature. This poses a challenge to both engineers and scientists. In terms of engineering applications, amorphous solids lack the capability of plastic deformation without fracture under ambient conditions, severely limiting the manufacture and utility of glasses. For example, there is currently a relentless push to make metallic glasses (MGs) ductile at RT so that their use in structural applications can be widened [10]. From the standpoint of materials science, an interesting question to explore is how to facilitate bond breaking and re-forming in the amorphous structure, to mimic viscous flow at elevated temperatures (or the action of dislocations in crystalline solids). Our current understanding with regard to how to tailor the amorphous structure of glassy materials to enable flow under applied loads is so far in its rudimentary stage, especially when compared with the well-established microstructure-plasticity relations in crystalline materials.

In this Perspective, we draw the attention of the community to recent experimental observations of glassy solids that have been made ductile at RT; we will cite one example (Cu-Zr) as a representative for metallic glasses (MGs), and one (amorphous silica) for covalent network glasses. While the examples may be extreme cases, we use them to advocate our perspective that if the amorphous structure can be made unusually flexible to facilitate bond switching in shear transformations, glasses can all be rendered to flow at RT. The focus of this article is molecular

CONTACT Evan Ma ema@jhu.edu Department of Materials Science and Engineering, Johns Hopkins University, Baltimore, MD 21218, USA

Supplemental data for this article can be accessed here. https://doi.org/10.1080/21663831.2018.1503198

© 2018 The Author(s). Published by Informa UK Limited, trading as Taylor & Francis Group
This is an Open Access article distributed under the terms of the Creative Commons Attribution License (http://creativecommons.org/licenses/by/4.0/), which permits unrestricted use, distribution, and reproduction in any medium, provided the original work is properly cited.

dynamics (MD) simulation results, which, coupled with these experimental examples, reveal the origin of the ductility achieved. Our thesis is that the flexibility affordable by the atomic bonding and local configurational environment, rather than the sheer magnitude of excess spatial volume (local free volume), quantitatively determines the shear modulus, which scales with the energy barrier for relaxation [14], and hence controls the (local) propensity for shear transformations. This causal correlation will be demonstrated to be universal for both metallic glasses and covalently bonded glasses. The case studies we discuss in the following also suggest processing strategies that can enhance the flexibility in the amorphous structure, in particular through the retention of, or structural rejuvenation to restore, sufficient heterogeneous liquid-like regions with high flexibility.

2. Glasses made ductile at room temperature

To set the stage for our discussion of the relationship between structural flexibility and deformability, we first cite experimental examples of glasses made ductile at RT. This is only for brief demonstration purposes, since our emphasis is on the structural origin underlying the flow.

2.1. Metallic glasses

There have been a number of recent experimental observations of MGs exhibiting tensile ductility at RT [15]. Figure 1 is a representative case, demonstrating that 'normal-metal-like' behavior is indeed possible for an MG at RT [16,17]. This engineering stress–strain curve of $Cu_{49}Zr_{51}$ MG is fully quantitative, showing an apparent elastic regime, followed by yielding and some uniform elongation accompanying apparent strain hardening, to a rather high tensile strength of $\sim$2.5 GPa (at a strain around 4.6%), where progressive necking starts. The total elongation is $\sim$10%. This tensile strain to failure, and the eventual cone-like shape of the fractured region, is typical of conventional ductile alloys that experiences necking in a uniaxial tensile test. Such a ductile behavior is achieved because the glass sample size is very small (see inset of Figure 1), such that it contains no pre-existing nuclei or easy nucleation sites for shear bands. Also, the small sample volume stores limited elastic strain energy and provides only a short runway, such that strain fluctuation across the sample does not get to develop into severe shear localization that evolves into a mature shear band [16,17]. We note that in this particular case, the $Cu_{49}Zr_{51}$ MG sample was prepared using melt spinning, such that rapid quench was involved, and the glass structure was further rejuvenated during the cutting of the test specimen using focused ion beam [16,17].

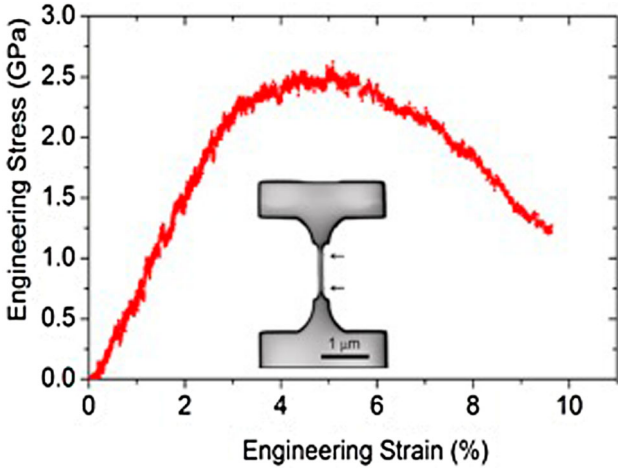

Figure 1. Engineering stress–strain curve of $Cu_{49}Zr_{51}$ MG. The inset shows the sample used in the *in situ* test. The arrows point to the gauge section. The high strength ($\sim$2.5 GPa) observed indicates that the temperature cannot be much higher than RT. Adapted from Ref. [17].

Irradiation of MGs using ion beam was also used recently by several other groups [18–21], and found to promote ductility. As will be discussed later, this is an effective approach to impart flexibility into the glass structure. One can also use rapid quench to retain flexibility from the parent phase, such as vapor-quench via sputter deposition, to produce Zr-Cu-Al thin films that are ductile in tension [22]. Our discussions later will cover both routes, rapid quench (from the liquid) as well as irradiation (by disposing extra energy to atoms), in our MD models.

2.2. Covalently bonded network glasses

Covalently bonded network glasses are well known to be completely brittle at RT. It is therefore somewhat surprising to observe in Figure 2 that an amorphous silica (a-SiO_2) ball can be compressed into a pancake without

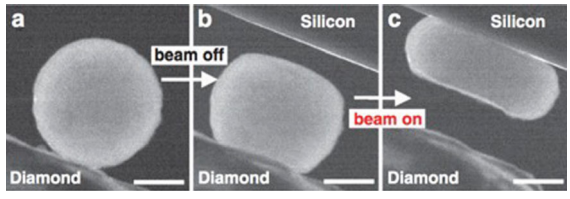

Figure 2. Compression of a-SiO_2 ball inside an electron microscope. Panels (a)–(c) show the centered dark-field images. In (a), the ball is adhered to the diamond punch and the silicon punch has not moved into the picture. In (b), the ball, after irradiation in (a), is imaged after it has been pressed with the beam off. Subsequently in (c), with the beam on, the ball can be compressed into a pancake without fracture or severe shear localization (shear banding) under a moderate force. The scale bar is 200 nm. Adapted from Ref. [23].

fracture or severe strain localization. This homogenous shape change clearly involves extensive plastic deformation. Nanowires of normally brittle amorphous silica in fact appeared superplastic in a tensile test inside a TEM [23]. Note that with the imaging e-beam on, the flow stress is a factor of three lower [23] than when the beam is blanked off, producing the pancake-shaped disk within two minutes. This shows that the e-beam dynamic rejuvenation during compression is more effective in making the silica flow than post-irradiation deformation.

We only briefly mention these two examples, one for metallic glasses and one for covalent glasses, because they suffice to motivate the focused discussions in this Perspective on the understanding as to what is happening in the amorphous structure that could make these glassy materials flow at RT. For a survey of making glasses ductile at RT, the readers are referred to Ref. [15], where it is seen that rapid quench and irradiation rejuvenation are often involved. We will, therefore, use modeling in Sections 3 and 4 to shed light on the changes in the glass structure processed via these two processing routes. In general, the overarching mechanism is the same: it is the retention of, or the rejuvenation to restore, flexibility in the glass structure that makes glass flow at RT upon loading.

3. Origin of ductility: flexibility versus excess volume

Glasses gain the ability of viscous flow at temperatures near or above the glass transition temperature, due to thermally activated bond switching that reposition and rearrange the atoms [24]. Then what does it take to make the same happen at RT? To answer this question, it is attempting to simply invoke the well-known concept of free volume, v_f [25], which is a widely cited structural parameter in the literature on glasses. On a per atom basis, v_f is the 'critical excess' [26] relative to a critical atomic volume corresponding to a reference glass state that has zero free volume. A popular answer to the question we posed above, in numerous papers over the years, is to add more free volume into the glass. v_f increases the extra space needed for dilatation during shear transformation, and as a result renders the glass more deformable [27].

However, this free volume concept is more appropriate for hard sphere models and polymeric glasses, but deficient for describing much softer inter-atomic potentials [28]. The latter also leads to ambiguous or inaccessible reference state [29], making v_f difficult to identify and quantify. In the literature, the more easily measurable average atomic volume Ω_a (or Voronoi cell volume, or the volume/density difference from the corresponding crystal) is often used to reflect the free volume content, because the Ω_a is expected to scale with the v_f. In the following, we will use case studies related to our examples in Section 2, to illustrate the inadequacy of the free volume picture and advocate a flexibility concept that can explain all the ductility trends observed.

3.1. Elevating flexibility to make MGs ductile

We begin our discussion with the MGs, as it is a case for which the origin of ductility has often been perceived to be well known. Different from covalent network glasses characterized by localized directional bonds, where the free volume idea is obviously not applicable (see Section 3.2), so far most publications in the MG community have embraced the free volume idea, often using Ω_a as the indicator. A rapidly quenched MG is believed to contain more free volume than a slowly cast one and is thus less rigid and more prone to flow [30,31]. An often-mentioned reason to resort to the volume-centric Ω_a is that MGs have densely packed amorphous structure, so the presence of excess spatial volume would be important to allow dilatation to instigate shear transformation [27].

However, despite of the frequent citing of v_f (Ω_a), most researchers in the community are aware of the drawbacks with this parameter. This is because v_f is not quantifiable as the reference zero-v_f state is not well defined [32,33]. Even the measurable Ω_a is not user-friendly, as it is insensitive to composition and processing history of MGs. Here we use MD simulations employing the LAMMPS code [34] and EAM potential [35], to compare MGs at the same $Cu_{64}Zr_{36}$ composition. Even when the shear modulus (G) differs by 30% due to different processing history (cooling from the liquid with rates of 1×10^9 to 1×10^{13} K/s), the difference in Ω_a is miniscule (15.9043 versus 16.0159 Å^3, 0.7%) [36], as shown in Figure 3. Also, in correlating with deformation kinetics, Ω_a does not quantitatively determine any activation parameter. Moreover, even if we assume one can figure out how much change of v_f has happened in the sample, e.g. it has increased by 1%, it is still not possible to predict how much change in properties would be induced. It is therefore difficult to use Ω_a to explain the MG ductility seen in Figure 1.

This calls for a new parameter, one that can be quantitatively determined and sensitive to processing. We recently defined such a parameter, termed flexibility volume [36],

$$v_{\text{flex}} = \frac{\langle r^2 \rangle}{a^2} \cdot a^3 = \langle r^2 \rangle \cdot a, \tag{1}$$

where $\langle r^2 \rangle$ is the vibrational mean squared displacement (MSD) and a is the average atomic spacing. Both are temperature dependent so Equation (1) is a quasi-harmonic

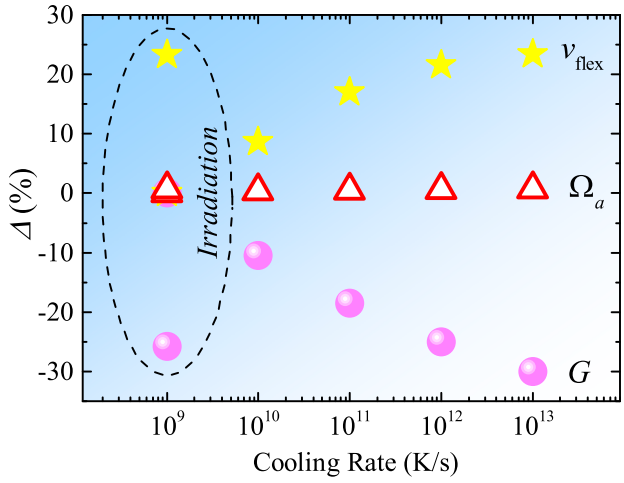

Figure 3. Percent change (Δ) of modulus (*G*), atomic volume (Ω_a) and flexibility volume (v_{flex}) for $Cu_{64}Zr_{36}$ MGs with various processing history (cooling rates and irradiation), relative to the corresponding values for the sample quenched at cooling rate of 1×10^9 K/s. Note that *G* decreases while v_{flex} increases with faster cooling rates or after irradiation. The increase in Ω_a. is too small to be meaningful.

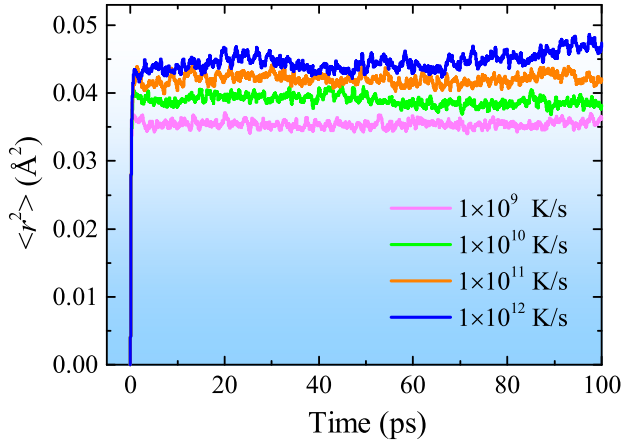

Figure 4. Evaluation of the vibrational mean squared displacement (MSD), i.e. $\langle r^2 \rangle$, for $Cu_{64}Zr_{36}$ MGs prepared using various cooling rates. The magnitude of MSD is dependent on processing (cooling rate)

approximation. v_{flex} can be viewed as an effective free volume, by modifying local atomic volume with the Lindemann ratio. Specifically, v_{flex} combines static atomic volume with dynamics information, through the MSD, which is readily evaluated in the MD model, see an example in Figure 4. In other words, v_{flex} uses vibration-assessed wiggle room as a probe to 'test the water', to gauge how flexible the local configuration is, under the particular geometrical and bonding environment.

Importantly, v_{flex} quantitatively correlates with *G* [36,37], as shown in Figure 5. It is significant that this correlation is deterministic, because *G* is known to scale

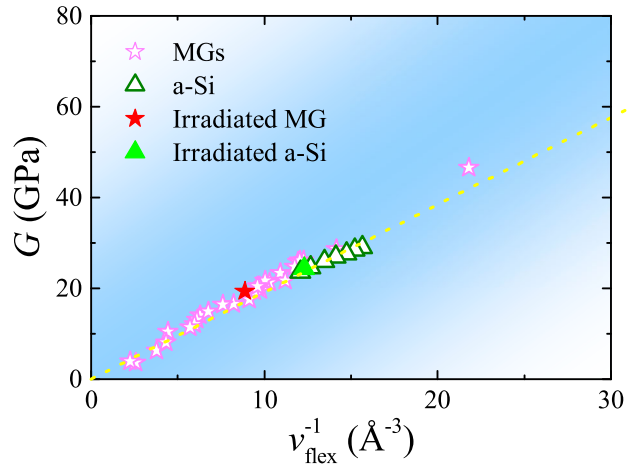

Figure 5. Correlation between shear modulus (*G*) and flexibility volume (v_{flex}) for both MGs and a-Si, including after experienced irradiation. Data of non-irradiated MGs and a-Si were adopted from Ref. [36] and [37], respectively.

with the activation energy for thermally activated relaxation and the propensity for stress-driven shear transformations [14]. *G* also scales with the yield strength [38].

As seen in Figure 3, the absolute percent change of v_{flex} is comparable to that of *G*, a clear advantage over the indistinguishable Ω_a in the same figure. From the shift of the sample-average v_{flex} by ~25%, one expects a similar percent change in *G* and a corresponding change in strength. This quantitative correlation is a clear advantage over other previously used parameters such as free volume, fictive temperature [39,40], topological disorder (GUMs [41,42]), soft spots [43–45], or liquid-like flow defects [46,47]. Figure 6 displays the stress–strain curves in uniaxial tension at 50 K for $Cu_{64}Zr_{36}$ MG obtained by cooling at 1×10^{10} and 1×10^{13} K/s from the liquid. The 1×10^{10} K/s sample shows an overshoot stress to rejuvenate the structure for initial yielding, followed by a major stress drop on the curve, which is a signature of strain localization [48,49]. This is in contrast with the 1×10^{13} K/s sample, showing no overshoot and sustainable plastic flow.

As such, v_{flex} gets around several shortcomings with free volume, particularly its vague and non-quantitative nature. In particular, v_{flex} allows a direct comparison of the structural flexibility after different processing, making it very useful to explaining the strength/ductility behavior such as the prediction of the corresponding change in modulus, strength and uniformity of flow. For the latter, the higher the v_{flex}, the lower the local *G*, the lower the activation barrier for shear transformations, and hence an easier and more spread-out flow. This can be rationalized by assuming that the plastic flow is proportional to the propensity for (or the rate of) shear flow,

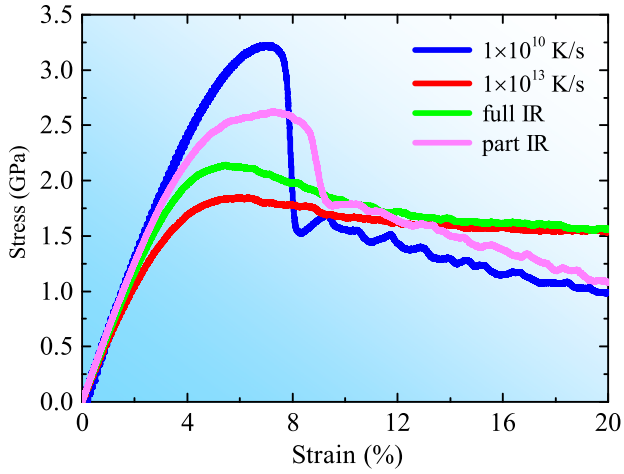

Figure 6. Stress–strain curves in uniaxial tension (along Z-direction) loaded at 50 K with constant strain rate of 4×10^7 s^{-1} for $Cu_{64}Zr_{36}$ MGs with various processing history (full IR: irradiated entire sample; part IR: irradiated X surfaces of the sample). Those samples have dimensions of 40.1 (X) × 8.0 (Y) × 79.5 (Z) nm^3, containing 1.6 million atoms. Periodic boundary condition (PBC) was imposed in the Y- and Z-directions, while free surface was used in the X-direction to allow shear offset on the free surfaces.

P, which in turn is controlled by $G\ (= Ck_BT/\upsilon_{flex})$ [36] in the energy barrier for shear flow,

$$P = P_0 \exp\left(-\frac{\alpha C}{\upsilon_{flex}}\right), \tag{2}$$

where α scales with an activation volume and is composition dependent. With υ_{flex} increasing via rapid quench and/or irradiation, the probability for shear transformation increases, assuming the prefactor and activation volume remain similar for samples at the same composition.

Indeed, there is almost no stress overshoot in the curve of the 1×10^{13} K/s sample. The glass structure is ready to flow, and after yielding the smooth flow stress plateau suggests stable homogeneous plastic deformation. A direct comparison showing the strain distribution in the sample is presented in Figure 7 for the samples strained to 20% in uniaxial tension. The contrasting behavior of the two MGs is evident. In contrast to the high υ_{flex} case of the 1×10^{13} K/s sample, where shear transformations spread out uniformly throughout the sample, υ_{flex} is inadequate in the 1×10^{10} K/s sample, exhibiting inhomogenous deformation. Strains localize into a single dominant shear band quickly as a result, as contrasted in Figure 7 (upper panel vs. lower panel), and in Movies 1(a, b, c) and 2 (see Supplementary Materials).

Again the drastic difference in plastic flow is attributable to the difference in υ_{flex} after cooling at the two different rates: this can be seen by comparing the atomic υ_{flex} in the probability distribution compared in Figure 8 for the two cooling rates. The sample with a faster cooling rate has much more local regions with larger υ_{flex} compared to the sample with the slower cooling rate. These local regions are fertile sites where shear transformation zones (STZs) prefer to emerge (see Section 4 for further evidence). Such spread-out fertile sites help to distribute the strain to avoid localization into a single severe shear band, as shown in Figure 7.

Another way to elevate the υ_{flex} of an MG is to irradiate the sample with the energetic beam. Note that Ω_a remained almost unchanged (15.9043 vs. 16.0104 $Å^3$, 0.67%) even after full irradiation of the 1×10^9 K/s sample. The sample-average υ_{flex}, on the other hand, increased by 23%, to the level equivalent to the 1×10^{13} K/s sample, as shown in Figure 3. And the distribution also approaches that of the latter, see Figure 8. The stress–strain curve (included in Figure 6) and the distribution of local strain (not shown) also become similar to that of the 1×10^{13} K/s sample. Similar irradiation effects on MG ductility were reported by Shi et al. [50] and Albe et al. [51].

In addition to fully irradiating the MG samples as did by Albe et al. [51], we also irradiated the free surface normal to the X-direction of $Cu_{64}Zr_{36}$ MG sample, similar to the simulation of Shi et al. [50] on cylindrical MG samples with a small radius of 3.9 nm. Our work used much larger samples containing 1.6 million atoms: for saving computing time, we first duplicated small cubic sample quenched at cooling rate of 1×10^9 K/s containing 32,000 atoms and cell length of $\sim$ 8 nm (5× along the X-direction), and then opened free surfaces (PBCs for the other two). To simulate the irradiation, on each X free surface a randomly chosen atom < 12 nm from the free surface was taken as the primary knock-on atom (PKA). A velocity parallel to the X-direction is assigned to this atom: the corresponding recoil energy (kinetic energy) is 10,000 eV when the PKA is at the open surface, linearly decreasing to 100 eV at 12 nm. The collision cascade process is similar to that in Ref. [50]. After enough cascade loops when the energy and υ_{flex} become steady, the sample was duplicated along the Z-direction by a factor of 10 and relaxed for 1 ns at RT before the final quench to 50 K. Its stress–strain curve in Figure 6 shows apparent work-hardening (bending of the curve after yielding), very similar to that observed in Figure 1 (the evolution can be seen in Figure 7 and Movie 3). From the contrast shown in Figure 9, it appears that the gradual exhaustion of the rejuvenated υ_{flex} in the irradiated layer, rather than the annihilation of Ω_a, is responsible for the work-hardening observed.

In sum, flexibility volume can be retained via faster quench, and a similar level can also be reached via rejuvenation (irradiation) of a slower cooled (or relaxed) sample (Figures 3 and 8). These explain the evenly distributed

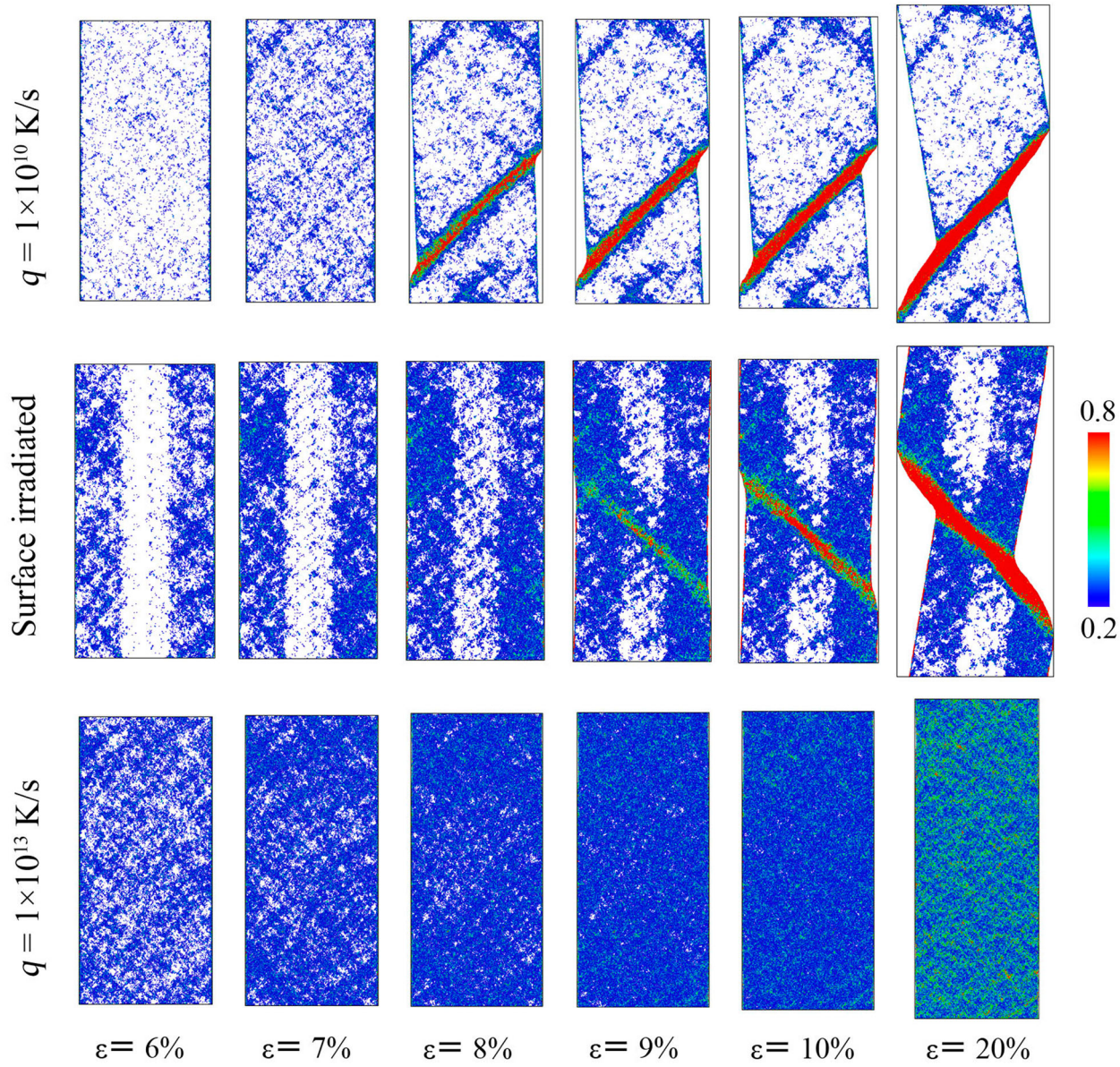

Figure 7. Projected views of the atomic configurations, showing the deformation process corresponding to Fig. 6, by monitoring local shear strain of each atom for $Cu_{64}Zr_{36}$ MGs quenched at cooling rate (q) of 1×10^{10} K/s (upper panel), 1×10^{9} K/s followed by surface irradiation (middle panel), and 1×10^{13} K/s (lower panel), respectively. Only atoms with a local shear strain above 0.2 are shown.

flow observed in Figure 7, and the experimental observation in Figure 1.

3.2. Flexibility makes covalent network glasses ductile

We next explain the ductile flow of amorphous silica in Figure 2, again from the flexibility perspective. Such a covalently bonded glass is in fact an example for which the 'free volume' concept is utterly inapplicable. To make our point, in this section we will discuss MD-simulated models of amorphous silicon (a-Si), as a general case study of covalently bonded network glasses (for which amorphous silica and a-Si are typical examples). a-Si has a coordination number ~ 4 and an open structure to begin with. But the ample 'empty space' is apparently not tantamount to easy flow, and introducing even more spatial volume into the structure makes little difference.

This brings us to the following question: other than spatial volume for dilatation, what else is essential to enable bond switching to mediate shear transformations? As seen in the schematic in Figure 10, the relocation of the atoms in the shear transformation requires bond breaking and re-forming, so the formation of dangling bonds and weakening of the rigid covalent bonds would be a particularly important pre-requisite for bond

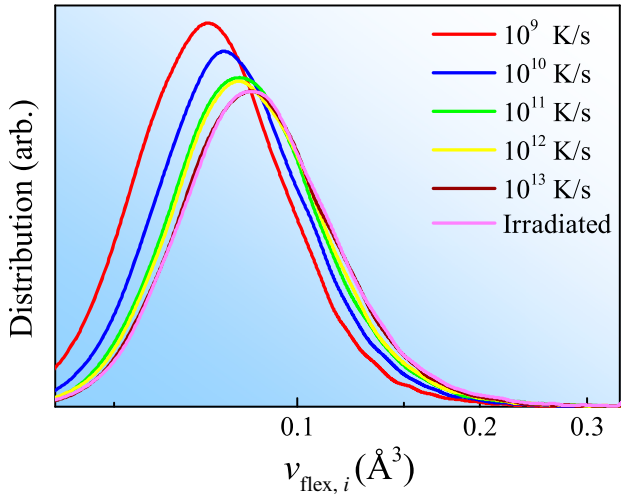

Figure 8. Probability distribution of the atomic flexibility volume ($v_{\text{flex},i}$)of $Cu_{64}Zr_{36}$ MGs with various processing history (cooling rates and irradiation).

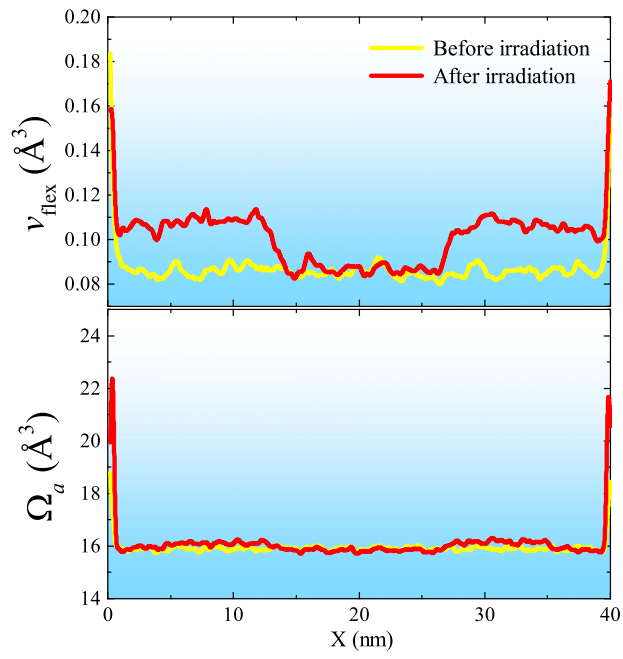

Figure 9. Contrast of the distribution of flexibility volume (v_{flex}) (upper panel) and atomic volume (Ω_a) (lower panel) along the X-direction of $Cu_{64}Zr_{36}$ MG before and after irradiation on the X-free surfaces.

switching. Without this bonding flexibility, shear transformation does not happen readily, despite of the open space surrounding the tetrahedrally bonded motifs. Just like the MG case, MSD can be sent as a 'detective' that gets down to near the bottom of the energy basin to sense the curvature, i.e. the flatness of the basin and the bond force constant. In other words, v_{flex} once again serves the purposes of gauging the flexibility available.

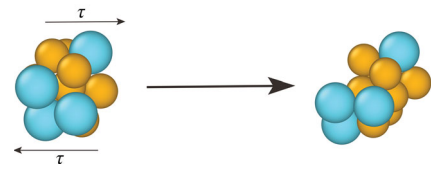

Figure 10. A schematic of the local shear transformation of a group of atoms.

Here, the SW a-Si model [37,52] is used to illustrate our point of view. We are aware that there are other potentials developed to model a-Si (e.g. a modified SW potential with doubled three-body term to increase the degree of bond directionality and thus the stiffness, plus quenching at a constant density with the Tersoff potential [53–55]), especially since the SW a-Si model tends to exhibit much more ductility than experimental a-Si in the laboratory [56,57]. For amorphous silica there has also been much potential development, including ongoing efforts [58]. However, we choose to use the simpler SW potential as a model, which suffices to deliver our main point at a low computational budget. Our message would not depend on the potential used, and the model material is only used to show that the ample space or excess volume available in the open glass structure is insufficient to sustain ductility by itself. The difficulty with plastic flow lies instead in the unforgiven chemical bonds that suffocate the flexibility to realize bond switching.

Figure 11 shows the stress–strain curves in uniaxial (pulling along the Z-direction) tension. We observe that the a-Si cooled at 5×10^{10} K/s requires an overshoot stress of ~ 5 GPa to initiate flow, followed by obvious localization of plastic strain into very narrow bands as can be seen in Figure 12(a) after straining to 20%.

We now show what can be done to make a-Si more amenable to plastic deformation. One way is to quench the liquid at rapid rates, e.g. 5×10^{13} K/s in Figure 11 for SW a-Si. The stress overshoot is eliminated, indicating that the as-quenched glass structure becomes ready to flow, and the flow stresses are also cut by more than half when compared with the slower cooled glasses. The strain localization is also replaced by distributed flow, as compared in Figure 12(b). In other words, just like MGs, we see that by increasing the quench speed from the liquid, a-Si can indeed be made easier to flow and in a more uniform manner.

Now, it is important to note that, the Ω_a in the SW a-Si glasses is actually decreasing with increasing quench rate, as demonstrated in Figure 13, while the glasses become more amenable to flow. It is thus obvious that more spatial volume is not the enabling condition for easier flow. Rather, the bonding at the higher quench rate contains

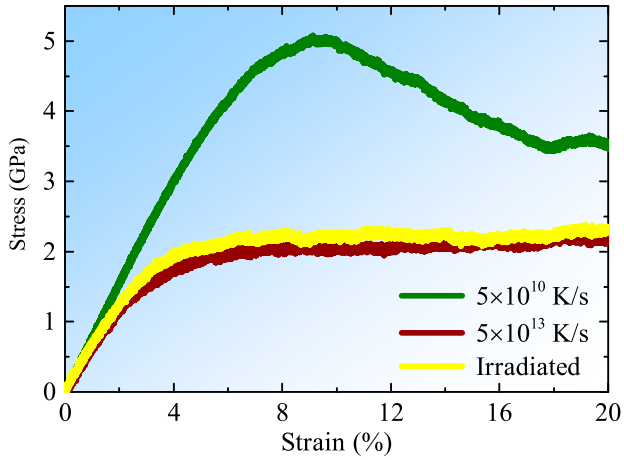

Figure 11. Stress–strain curves in uniaxial tension (along Z-direction) loaded at 300 K with constant strain rate of 1×10^8 s^{-1} for SW a-Si with PBCs in all three directions and quenched at cooling rate of 5×10^{10} and 5×10^{13} K/s and one after irradiation. The stress normal to the loading direction was relaxed to allow for lateral contraction.

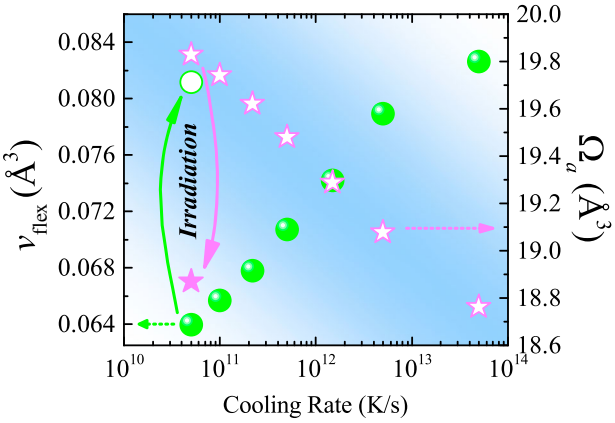

Figure 13. Variation of flexibility volume (v_{flex}) and atomic volume (Ω_a) of SW a-Si due to different processing history (cooling rates and irradiation).

more metallic character (and therefore higher coordination number and mass density [46,47]), such that the amorphous structure is more flexible for plastic flow despite of the reduction in average atomic volume.

The second route to make glasses ductile is to rejuvenate the already-relaxed amorphous structure. We model this by irradiating the 'slowly' (5×10^{10} K/s) cooled SW a-Si sample. In simulating the irradiation, the short-range repulsion of the SW potential was modified with the Ziegler–Biersack–Littmark (ZBL) potential [59], with a spline function joining with SW [60]. Each cascade was initiated by giving a random primary knock-on atom (PKA) a recoil energy of 4 KeV in a random direction. The simulation time for each cascade run was 20 ps under an NVE ensemble. Following each cascade run, a relaxation run was carried out under an NPT ensemble with the cooling rate of 1×10^{13} K/s, decreasing the system's temperature and pressure to 300 K and 0 bar, respectively. After 150 such loops, we observe in Figure 11 that the irradiated glass shows a stress–strain curve very close to the 1×10^{13} K/s quenched sample. The strain localization in Figure 12(a) is also alleviated, as seen in Figure 12(c). Interestingly, as shown in Figure 13, the Ω_a is actually reduced after irradiation, consistent with the densification reported in previous irradiation studies on amorphous silicon and silica [61]. This demonstrates once again that the spatial free volume picture is not generally applicable as a universal explanation to making glasses ductile.

Next, we show that in this case the flexibility in the amorphous structure remains a powerful indicator to rationalize the deformation readiness. We first note that, even though our a-Si model is a covalently bonded network amorphous material qualitatively different from the metallically bonded and densely packed MGs for which v_{flex} was first demonstrated, the v_{flex}-G correlation in Figure 5 remains valid. This shows v_{flex} is a universally applicable indicator of the rigidity for different

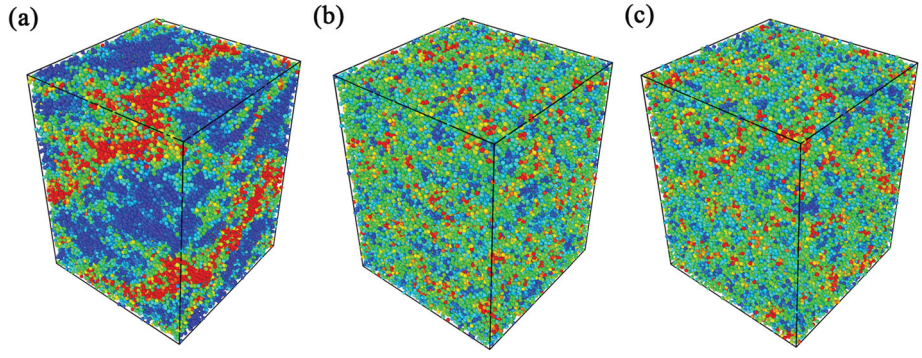

Figure 12. Snapshots of SW a-Si with various processing history were strained to 20% in uniaxial tension at 300 K. Color represents the local shear strain of each atom (red and blue represent upper and lower limit, respectively). Panels (a) and (b) are as-quenched samples with cooling rate of 5×10^{10} and 5×10^{13} K/s, respectively; (c) is irradiated as-quenched samples with cooling rate of 5×10^{10} K/s.

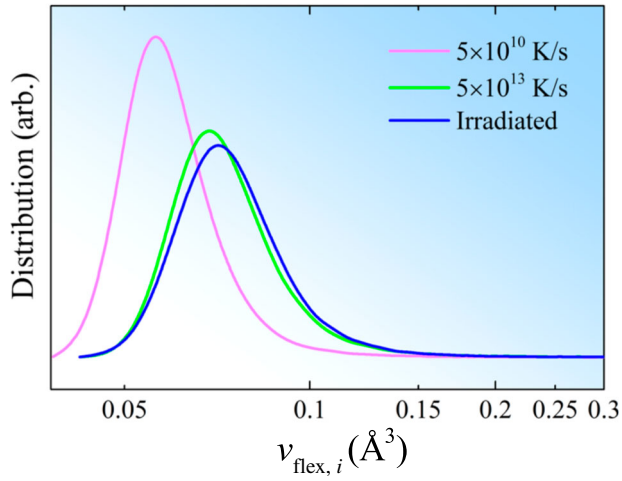

Figure 14. The probability distribution of the atomic flexibility volume ($v_{flex,i}$) in SW a-Si with different processing history.

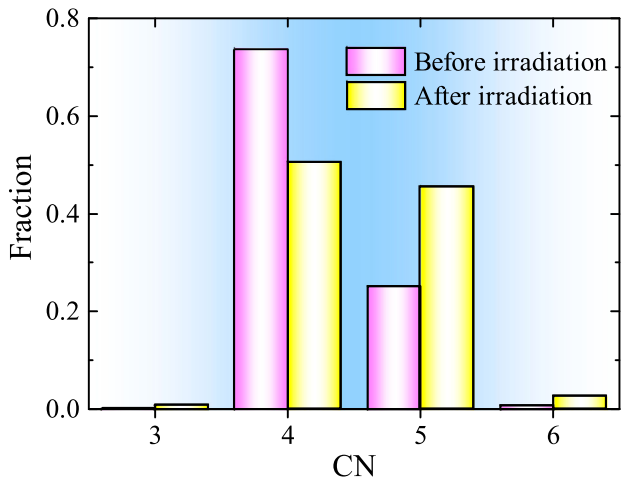

Figure 15. The change of coordination number (CN) of a-Si due to irradiation.

types of glasses, even for the 'denser is more deformable' cases.

The faster the quench from liquid, the larger the v_{flex}, as shown in Figure 13. This signals a smaller G as seen in Figure 5 and reduced energy barrier for inelastic relaxation. The irradiated SW a-Si, while denser with Ω_a decreased (Figure 13), also arrives at an elevated v_{flex} (Figure 13) and in turn a reduced G (Figure 5), both similar to that in the fastest quenched glass (including an obvious shift of the distribution of v_{flex}, Figure 14). So we again conclude that it is the higher flexibility retained or rejuvenated in the amorphous structure that renders the resultant glass more amenable to shear flow [46,62]. The excess volume or open structure is inconsequential in determining the deformability.

The increased flexibility with reduced atomic volume (or increased density) is due to the more metallic-like bonding retained from liquid Si via the rapid quench [46,47]. Figure 15 shows that after irradiation, the coordination number of Si shifts from CN = 4 dominated to CN = 5, suggesting the increased population of more liquid-like regions. This latter term was used by Demcowicz and Argon [46,47]; now 'liquid-like' region would mean a higher v_{flex} and lower G, both of which are quantifiable. These heterogeneities are shown in Figure 16. In the next section, we will confirm that the v_{flex} correlates well with the local atomic shear strain, as defined in Ref. [63] and calculated using the OVITO program [64].

We started in Section 2 with the example that the normally brittle amorphous silica turned very ductile (Figure 2) inside a TEM [23]. The arguments for a-Si above can also be used for amorphous silica, which behaves in many ways similar to a-Si, as another typical covalently bonded network glass. It belongs to the category where the free volume concept is not applicable. The high deformability that the a-SiO_2 ball can be compressed into a pancake is again due to the flexibility imparted into the structure, in this glass enabled by the electron beam irradiating on the sample, as it is being deformed inside an electron microscope. The e-beam illuminating on a-silica dynamically rejuvenates the glass structure, particularly effective when the deformation is carried out

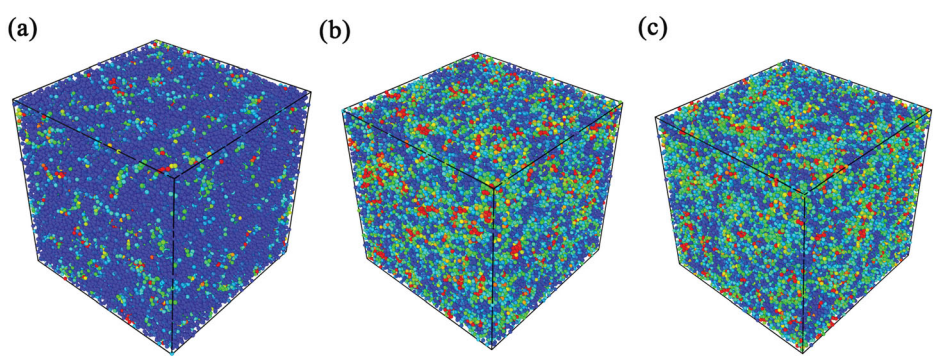

Figure 16. Spatial distribution of the atomic flexibility volume ($v_{flex,i}$) before tension of SW a-Si with various processing history. (a) and (b) are as-quenched samples with cooling rate of 5×10^{10} and 5×10^{13} K/s, respectively; (c) is the as-quenched samples with cooling rate of 5×10^{10} K/s after irradiation.

in situ when the sample is continuously imaged to monitor its deformation. The weakened bonds due to energy input under ionization irradiation have been found to be akin to ultrafast quench [61].

SiO_2 is highly susceptible to electron beam softening, such that the entire sample undergoing plastic deformation is constantly rejuvenated by e-beam irradiation, producing many simultaneous bond switching events to contribute to flow. We point out, however, that the exact mechanisms on the electron level that imparts flexibility may be more complicated than, what we have discussed above. For example, our simulation is about the direct breaking of bonds when the incident electrons transfer energy to Si, with a magnitude comparable to their displacement threshold energy, causing knock-on displacement and subsequent collision cascade. But there can also be other effects: e-beam with energies in the 0–100 eV range can cause radiolysis. Let us look at the silicon oxide case. Since all the valence electrons of Si are bound with O, there would be no spare ones left available to fill the Si core hole created by the electron irradiation (via intra-atomic Auger decay). Instead, O would have to return the electron lent from Si to accomplish an inter-atomic Auger process [65].

In any case, both mechanisms sever or weaken the bonding between O and Si and dynamically rejuvenate the silica glass structure, allowing bond breaking all over the sample volume under applied stresses [23]. Meanwhile, the strong and directional covalent bonds would quickly re-form with other neighbors. This bond switching is then akin to thermally activated bond breaking and re-forming in viscous flow at elevated temperatures. It provides the mechanism needed for shear transformations to produce strain and heal incipient damage, as the bond switching reconnects, reorients and relocates the SiO_4 motifs. The brittle silica glass is therefore made not only malleable in compression (Figure 2), but also ductile in tension at room temperature [52].

To recapitulate, in this section we have demonstrated three reasons as to why flexibility is the deciding factor towards plastic flow. First, flexibility is shown to explain the deformability trend, when the free volume is not appropriate to use at all, as seen for a-Si. Second, we also showed that at a glass composition, while Ω_a changes little with the different processing history of samples, ν_{flex} spans an appreciable range that can be tuned using different processing conditions. The third advantage is that ν_{flex} scales with G quantitatively (Figure 5), so one can directly connect it with the ease of inelastic relaxation (Equation 2) and compare glasses processed differently.

Note here that so far the discussion is, for the most part, about the sample-average ν_{flex}, correlating with the overall strength/ductility of a glass. One can in fact go one step further, to correlate with local atomic-level strains. Such details about local correlations will be discussed in the next section.

4. Correlating local flexibility with spatially heterogeneous shear transformations

Then, on the level of local atomic strain in glasses, does the local (coarse-grained on nanometer scale) ν_{flex} indeed indicate the propensity for shear transformations, which are expected to be heterogeneous and on the nanometer scale in the glass? In this section, we will confirm this heterogeneity and correlation, which is the fourth advantage of using flexibility, an important merit that Ω_a again fails to have. A strong correlation of atomic strains with local ν_{flex} but not with Ω_a will nail down our assertion in the preceding section that flexibility indeed has the ability to account for the readiness of shear transformation, and for the mechanical heterogeneities. We will also confirm that the correlation with local Ω_a is very weak. In fact, dense regions can be prone to shear transformations if their ν_{flex} is high.

It was shown in Ref. [36,37] that the magnitude of ν_{flex} correlates well with the fertile sites where shear transformations tend to take place in glassy materials under athermal quasistatic shearing [66]. Here we demonstrate that even under uniaxial tensile deformation at 300 K, which is typical in laboratory experiments, it is the ν_{flex}, and not the Ω_a, that is the meaningful marker of the propensity for shear transformations. To evaluate this correlation, we sort all atoms for each atom species in each sample ($Cu_{64}Zr_{36}$ and SW a-Si with various cooling history) into bins each containing 10% of all the atoms of that species, based on escalating flexibility volume ($\nu_{\text{flex,i}}$) or atomic volume ($\Omega_{a,\text{i}}$), and then count in each bin the fraction of atoms that have experienced the top 5% atomic strain when the overall uniaxial tensile strain was 3% (with PBCs along all three directions to eliminate the effect from atoms on free surfaces). The trend is clear in Figure 17(a, c and e) that the larger the coarse-grained ν_{flex} in a region, the larger the fraction of atoms with top 5% atomic strain, for both Cu and Zr atoms, respectively, in $Cu_{64}Zr_{36}$ MG, and for all the Si atoms in SW a-Si. In contrast, the propensity for shear transformation is almost the same for all bins sorted based on increasing $\Omega_{a,\text{i}}$, see Figure 17(b, d and f). In other words, atomic volume offers no useful information with regard to the likelihood of shear transformation. We also found that even at 20% overall sample strain, most atoms having relatively large atomic strain are still those with larger initial ν_{flex}. Figure 18 shows a map of Si atoms colored according to atomic strain in the 5×10^{10} K/s cooled SW a-Si

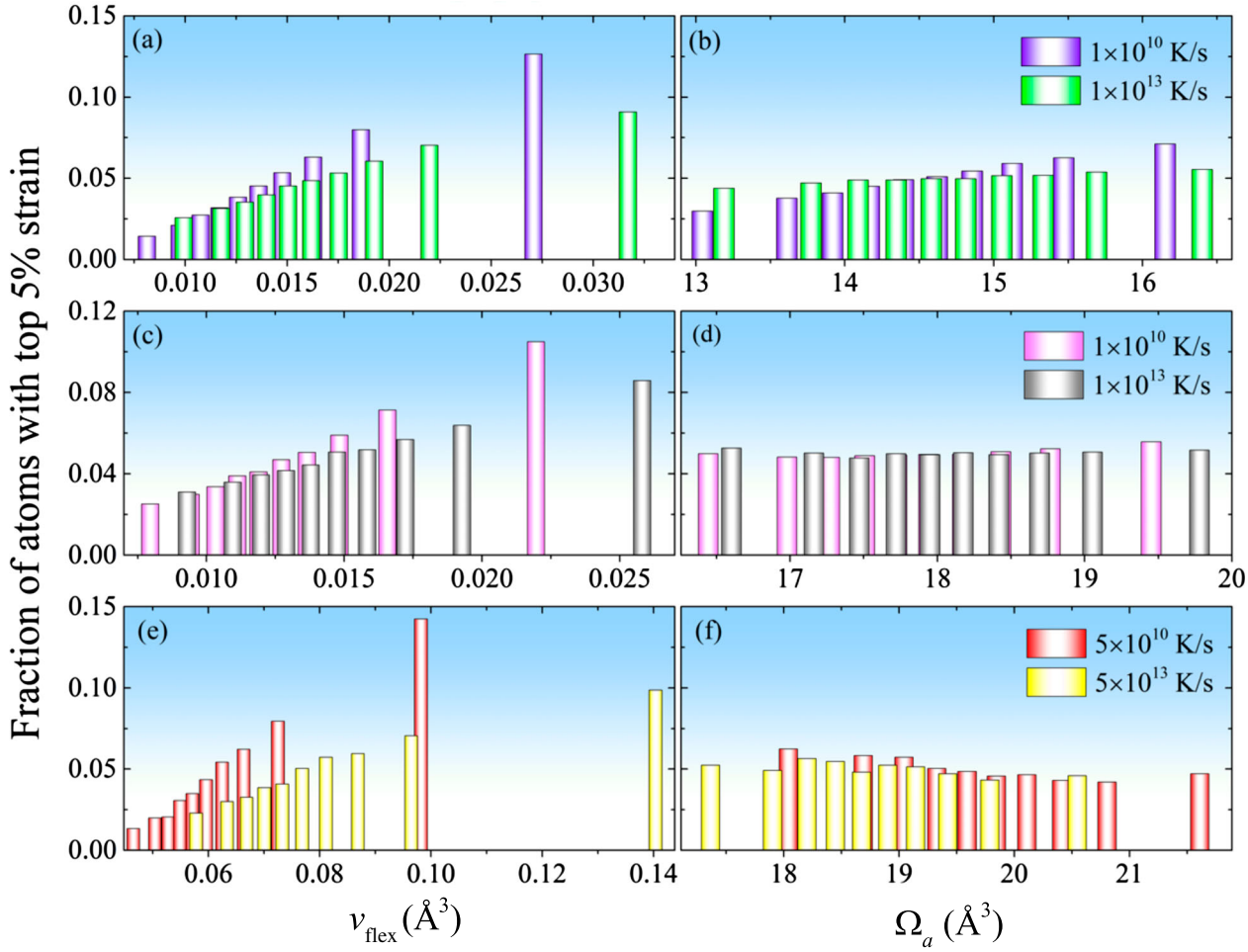

Figure 17. Correlating the flexibility volume (v_{flex})or atomic volume (Ω_a) with the propensity for shear transformations of atoms (fraction of atoms with top 5% atomic strain in each group when each sample was strain to 3% under uniaxial tensile deformation with PBCs along all three directions at 300 K). All the atoms of each atom specie in each sample are sorted based on flexibility volume ($v_{flex,i}$) or atomic volume ($\Omega_{a,i}$) into bins each containing 10% of all the atoms of each atom specie. Panels (a) and (c) show the correlation with v_{flex} for Cu and Zr atoms in $Cu_{64}Zr_{36}$ MG, respectively, and (e) shows the correlation with v_{flex} in SW a-Si. (b), (d) and (f) show that there is no observable correlation with Ω_a.

at 3% overall tensile strain. The three insets show the corresponding initial v_{flex} distribution in the three local regions circled. As clearly shown in the figure, the initial v_{flex} is larger in the region with more shear strain but smaller in the region with less shear strain, which confirms the correlation in Figure 17. These illustrate that flexibility volume can indeed serve as a tell-tale indicator to reflect the mechanical heterogeneity of amorphous materials, but local atomic volume cannot.

The flexibility is distributed heterogeneously in the glass [15,67,68]. So the flexibility imparted into the glass structure is consistent with the idea we advocated earlier [15], i.e. tailoring the amorphous structure to embed more heterogeneities and soft spots that are enriched with geometrically unfavored motifs (GUMs) [41,42]. Indeed, fast quench or irradiation are expected to retain more disorder and GUMs, which promote v_{flex} and aggregate into patches as structural heterogeneities that in turn produce spatial variations in v_{flex} and mechanical properties.

5. Concluding remarks on strategies to make glasses ductile

It follows from Section 4 that a higher population and density of high flexibility regions helps to carry imposed deformation and relieve strain localization. Although the cooling rates and strain rates used in our modeling are much faster than that in laboratory experiments due to the spatiotemporal scale limitation in current MD simulations, the trend discussed above should hold. That is, the more local regions with larger flexibility volume in a glass, the more ductile it would be. Glassy solids can all be made ductile at RT, if the amorphous structure is made sufficiently flexible.

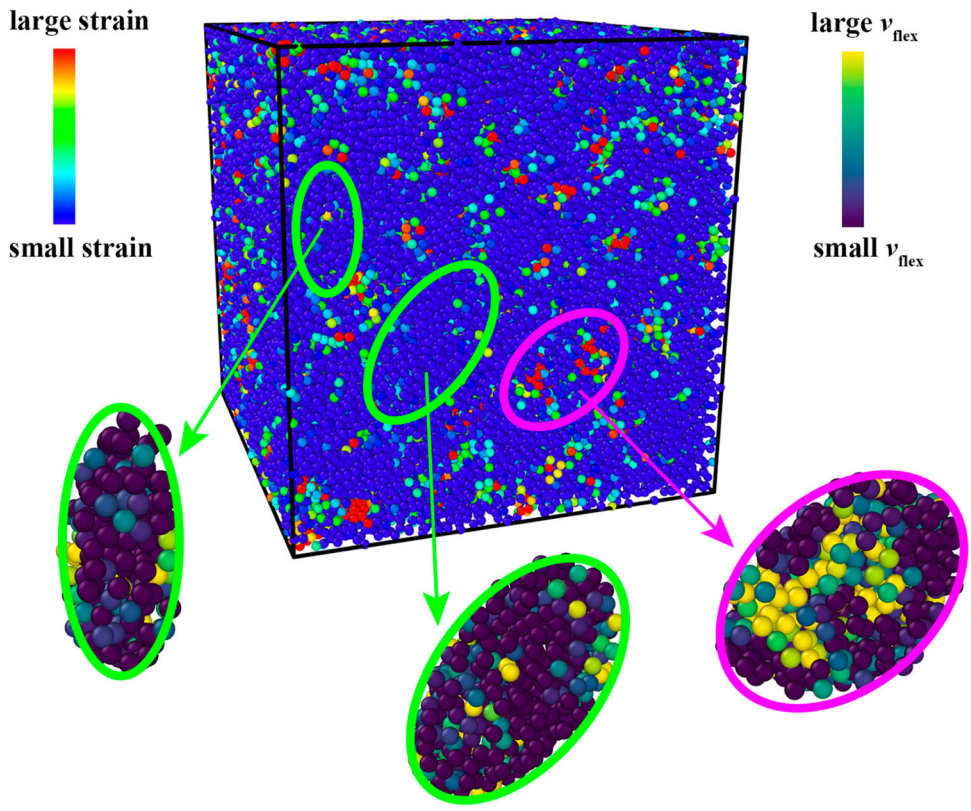

Figure 18. Atomic strain map when a SW a-Si with cooling rate of 5×10^{10} K/s was strained to 3% under uniaxial tensile deformation. The three insets show the corresponding flexibility volume (v_{flex}) distribution before deformation of three local regions.

Flexibility is about the propensity for bond switching upon loading and a high structural flexibility encourages spread-out shear transformations for plastic flow. For glasses a commonly used descriptor about structural flexibility is 'free volume', and glasses are likely to be more deformable if the free volume content is higher. This concept is, however, neither quantitative nor universal. There are several take-home messages from our discussions above. First, flexibility reigns, and an indicator of flexibility is the flexibility volume, not the local excess spatial volume, as shown above with an extreme case of open structure glasses such as amorphous Si and silica. They are made deformable only if the bonding is weakened to afford more flexibility, even though excess volume or elbow room for bond switching is always available. In other words, open space is a given but does not imply deformability. Second, flexibility volume v_{flex} can be quantified, and it quantitatively scales with shear modulus G to influence the relaxation energy barrier. Third, for MGs the variation is miniscule for Ω_a, but v_{flex} exhibits pronounced changes for different preparation history and for different compositions. With such a quantitative measure of flexibility, one can now compare glasses at a glass composition but processed differently, or different regions in a given glass (as a local measure of heterogeneous flexibility). Fourth, v_{flex}, easily obtained in MD simulations, provides a quantitative measure to reflect the overall effects of other indicators previously used in the glass community to correlate with deformation, such as fictive temperature, GUMs, liquid-like flow defects, soft spots, etc., each of which focusing on a certain aspect of the glass state/structure. Fifth and finally, the flexibility is non-uniform in glasses, able to account for mechanical heterogeneity. Of course, free volume is also heterogeneous, but shear transformation happens preferentially where flexibility is high, with no meaningful correlation with local atomic volume. This Perspective summarizes these major merits of using flexibility to describe the glass structure and its deformability; other advantages over Ω_a have been discussed before in Ref. [36].

We conclude that if adequate flexibility is activated throughout the sample, the deformation mode can become 'homogeneous'. To that end, one should retain flexibility from the parent phase to begin with, for example by rapid quench from liquid or vapor, or by using 'nanoglass', which consolidates glass nanoparticles together [49,69–71]. The other route we demonstrated is to rejuvenate an already-relaxed amorphous structure—irradiation appears to be an effective method

in that regard. Other rejuvenation routes including plastic deformation under triaxial stress state [72], elastoplastic loading [73] and cryogenic thermal cycling [74]; but they have yet to be shown to be effective in producing large deformability and tensile ductility. Generally speaking, the spread-out heterogeneities with high flexibility avoid the localization of plastic strains. The spatially distributed plastic events can then make glasses flow in a ductile manner at RT.

Disclosure statement

No potential conflict of interest was reported by the author(s).

Funding

This work was supported by U.S. DoE-BES-DMSE under grant DE-FG02-16ER46056 and NSF-DMR-1505621. J.D. was supported at the Lawrence Berkeley National Laboratory by the U.S. Department of Energy, Office of Basic Energy Sciences, Materials Sciences and Engineering Division, through the Mechanical Behavior of Materials Program (KC13) under Contract No. DE-AC02-05CH11231. The authors also acknowledge computational resources of the National Energy Research Scientific Computing Center (NERSC), supported by the Office of Basic Energy Sciences of the U.S. Department of Energy under contact No. DE-FG02-16ER46056.

References

[1] Greer AL. Metallic glasses. Science. 1995;267:1947–1953.
[2] Inoue A, Shen B, Koshiba H, et al. Cobalt-based bulk glassy alloy with ultrahigh strength and soft magnetic properties. Nat Mater. 2003;2:661–663.
[3] Duan G, Wiest A, Lind ML, et al. Bulk metallic glass with benchmark thermoplastic processability. Adv Mater. 2007;19:4272–4275.
[4] Zberg B, Uggowitzer PJ, Löffler JF. Mgznca glasses without clinically observable hydrogen evolution for biodegradable implants. Nat Mater. 2009;8:887–891.
[5] Greer AL, Ma E. Bulk metallic glasses: at the cutting edge of metals research. MRS Bull. 2007;32:611–619.
[6] Staebler DL, Wronski CR. Reversible conductivity changes in discharge-produced amorphous Si. Appl Phys Lett. 1977;31:292–294.
[7] Lin Y, Battaglia C, Boccard M, et al. Amorphous Si thin film based photocathodes with high photovoltage for efficient hydrogen production. Nano Lett. 2013;13:5615–5618.
[8] Hufnagel TC, Schuh CA, Falk ML. Deformation of metallic glasses: recent developments in theory, simulations, and experiments. Acta Mater. 2016;109:375–393.
[9] Schuh CA, Hufnagel TC, Ramamurty U. Mechanical behavior of amorphous alloys. Acta Mater. 2007;55:4067–4109.
[10] Greer AL, Cheng YQ, Ma E. Shear bands in metallic glasses. Mater Sci Eng R Rep. 2013;74:71–132.
[11] Sun BA, Wang WH. The fracture of bulk metallic glasses. Prog Mater Sci. 2015;74:211–307.
[12] Guo H, Yan PF, Wang YB, et al. Tensile ductility and necking of metallic glass. Nat Mater. 2007;6:735–739.
[13] Sehgal J, Ito S. Brittleness of glass. J Non-Cryst Solids. 1999;253:126–132.
[14] Johnson WL, Demetriou MD, Harmon JS, et al. Rheology and ultrasonic properties of metallic glass-forming liquids: a potential energy landscape perspective. MRS Bull. 2007;32:644–650.
[15] Ma E, Ding J. Tailoring structural inhomogeneities in metallic glasses to enable tensile ductility at room temperature. Mater Today. 2016;19:568–579.
[16] Tian L, Cheng Y-Q, Shan Z-W, et al. Approaching the ideal elastic limit of metallic glasses. Nat Commun. 2012;3:609.
[17] Tian L, Shan Z-W, Ma E. Ductile necking behavior of nanoscale metallic glasses under uniaxial tension at room temperature. Acta Mater. 2013;61:4823–4830.
[18] Magagnosc DJ, Ehrbar R, Kumar G, et al. Tunable tensile ductility in metallic glasses. Sci Rep. 2013;3:1096.
[19] Chen DZ, Jang D, Guan KM, et al. Nanometallic glasses: size reduction brings ductility, surface state drives Its extent. Nano Lett. 2013;13:4462–4468.
[20] Raghavan R, Boopathy K, Ghisleni R, et al. Ion irradiation enhances the mechanical performance of metallic glasses. Scr Mater. 2010;62:462–465.
[21] Thompson RL, Wang Y, Greer JR. Irradiation enhances strength and deformability of nano-architected metallic glass. Adv Eng Mater. 2018;0:1701055.
[22] Liontas R, Jafary-Zadeh M, Zeng Q, et al. Substantial tensile ductility in sputtered Zr-Ni-Al nano-sized metallic glass. Acta Mater. 2016;118:270–285.
[23] Zheng K, Wang C, Cheng Y-Q, et al. Electron-beam-assisted superplastic shaping of nanoscale amorphous silica. Nat Commun. 2010;1:24.
[24] Mott NF. The viscosity of vitreous silicon dioxide. Philos Mag B. 1987;56:257–262.
[25] Spaepen F. A microscopic mechanism for steady state inhomogeneous flow in metallic glasses. Acta Metall. 1977;25:407–415.
[26] Cohen MH, Turnbull D. Molecular transport in liquids and glasses. J Chem Phys. 1959;31:1164–1169.
[27] Spaepen F. Metallic glasses: must shear bands be hot? Nat Mater. 2006;5:7–8.
[28] Egami T. Atomic level stresses. Prog Mater Sci. 2011;56:637–653.
[29] Kirkpatrick TR, Thirumalai D, Wolynes PG. Scaling concepts for the dynamics of viscous liquids near an ideal glassy state. Phys Rev A. 1989;40:1045–1054.
[30] Cohen MH, Grest GS. Liquid-glass transition, a free-volume approach. Phys Rev B. 1979;20:1077–1098.
[31] Yavari AR, Moulec AL, Inoue A, et al. Excess free volume in metallic glasses measured by X-ray diffraction. Acta Mater. 2005;53:1611–1619.
[32] Widmer-Cooper A, Harrowell P. Free volume cannot explain the spatial heterogeneity of Debye–Waller factors in a glass-forming binary alloy. J Non-Cryst Solids. 2006;352:5098–5102.
[33] Manning ML, Liu AJ. Vibrational modes identify soft spots in a sheared disordered packing. Phys Rev Lett. 2011;107:108302.
[34] Plimpton S. Fast parallel algorithms for short-range molecular dynamics. J Comput Phys. 1995;117:1–19.
[35] Cheng YQ, Ma E, Sheng HW. Atomic level structure in multicomponent bulk metallic glass. Phys Rev Lett. 2009;102:245501.

[36] Ding J, Cheng Y-Q, Sheng H, et al. Universal structural parameter to quantitatively predict metallic glass properties. Nat Commun. 2016;7:13733.
[37] Fan Z, Ding J, Li Q-J, et al. Correlating the properties of amorphous silicon with its flexibility volume. Phys Rev B. 2017;95:144211.
[38] Johnson WL, Samwer K. A universal criterion for plastic yielding of metallic glasses with a $(T/T_g)^{2/3}$ temperature dependence. Phys Rev Lett. 2005;95:195501.
[39] Haxton TK, Liu AJ. Activated dynamics and effective temperature in a steady state sheared glass. Phys Rev Lett. 2007;99:195701.
[40] Kumar G, Neibecker P, Liu YH, et al. Critical fictive temperature for plasticity in metallic glasses. Nat Commun. 2013;4:1536.
[41] Ma E. Tuning order in disorder. Nat Mater. 2015;14: 547–552.
[42] Ding J, Patinet S, Falk ML, et al. Soft spots and their structural signature in a metallic glass. Proc Natl Acad Sci. 2014;111:14052–14056.
[43] Widmer-Cooper A, Perry H, Harrowell P, et al. Irreversible reorganization in a supercooled liquid originates from localized soft modes. Nat Phys. 2008;4: 711–715.
[44] Widmer-Cooper A, Perry H, Harrowell P, et al. Localized soft modes and the supercooled liquid's irreversible passage through its configuration space. J Chem Phys. 2009;131:194508.
[45] Mosayebi M, Ilg P, Widmer-Cooper A, et al. Soft modes and nonaffine rearrangements in the inherent structures of supercooled liquids. Phys Rev Lett. 2014;112: 105503.
[46] Demkowicz MJ, Argon AS. High-density liquidlike component facilitates plastic flow in a model amorphous silicon system. Phys Rev Lett. 2004;93:025505.
[47] Demkowicz MJ, Argon AS. Liquidlike atomic environments act as plasticity carriers in amorphous silicon. Phys Rev B. 2005;72:245205.
[48] Cao AJ, Cheng YQ, Ma E. Structural processes that initiate shear localization in metallic glass. Acta Mater. 2009;57:5146–5155.
[49] Albe K, Ritter Y, Şopu D. Enhancing the plasticity of metallic glasses: shear band formation, nanocomposites and nanoglasses investigated by molecular dynamics simulations. Mech Mater. 2013;67:94–103.
[50] Xiao Q, Huang L, Shi Y. Suppression of shear banding in amorphous ZrCuAl nanopillars by irradiation. J Appl Phys. 2013;113:083514.
[51] Avchaciov KA, Ritter Y, Djurabekova F, et al. Effect of ion irradiation on structural properties of Cu64Zr36 metallic glass. Nucl Instrum Methods Phys Res Sect B Beam Interact Mater At. 2014;341:22–26.
[52] Stillinger FH, Weber TA. Computer simulation of local order in condensed phases of silicon. Phys Rev B. 1985;31:5262–5271.
[53] Talati M, Albaret T, Tanguy A. Atomistic simulations of elastic and plastic properties in amorphous silicon. Europhys Lett. 2009;86:66005.
[54] Fusco C, Albaret T, Tanguy A. Role of local order in the small-scale plasticity of model amorphous materials. Phys Rev E. 2010;82:066116.
[55] Albaret T, Tanguy A, Boioli F, et al. Mapping between atomistic simulations and Eshelby inclusions in the shear deformation of an amorphous silicon model. Phys Rev E. 2016;93:053002.
[56] Holland D, Marder M. Ideal brittle fracture of silicon studied with molecular dynamics. Phys Rev Lett. 1998;80:746–749.
[57] Holland D, Marder M. Erratum: ideal brittle fracture of silicon studied with molecular dynamics. Phys Rev Lett. 1998;81:4029–4029.
[58] Sundararaman S, Huang L, Ispas S, et al. New optimization scheme to obtain interaction potentials for oxide glasses. J Chem Phys. 2018;148:194504.
[59] Ziegler JF, Biersack JP. The Stopping and Range of Ions in Matter. Treatise Heavy-Ion Sci. Boston (MA): Springer; 1985. p. 93–129.
[60] Gärtner K, Stock D, Weber B, et al. Round robin computer simulation of ion transmission through crystalline layers. Nucl Instrum Methods Phys Res Sect B Beam Interact Mater At. 1995;102:183–197.
[61] Wootton A, Thomas B, Harrowell P. Radiation-induced densification in amorphous silica: A computer simulation study. J Chem Phys. 2001;115:3336–3341.
[62] Demkowicz MJ, Argon AS. Autocatalytic avalanches of unit inelastic shearing events are the mechanism of plastic deformation in amorphous silicon. Phys Rev B. 2005;72:245206.
[63] Shimizu F, Ogata S, Li J. Theory of shear banding in metallic glasses and molecular dynamics calculations. Mater Trans. 2007;48:2923–2927.
[64] Stukowski A. Visualization and analysis of atomistic simulation data with OVITO–the open visualization tool. Model Simul Mater Sci Eng. 2010;18:015012.
[65] Egerton RF, Li P, Malac M. Radiation damage in the TEM and SEM. Micron. 2004;35:399–409.
[66] Maloney CE, Lemaître A. Amorphous systems in athermal, quasistatic shear. Phys Rev E. 2006;74:016118.
[67] Zhu F, Nguyen HK, Song SX, et al. Intrinsic correlation between β-relaxation and spatial heterogeneity in a metallic glass. Nat Commun. 2016;7:11516.
[68] Hu YC, Guan PF, Li MZ, et al. Unveiling atomic-scale features of inherent heterogeneity in metallic glass by molecular dynamics simulations. Phys Rev B. 2016;93: 214202.
[69] Ritter Y, Şopu D, Gleiter H, et al. Structure, stability and mechanical properties of internal interfaces in Cu64Zr36 nanoglasses studied by MD simulations. Acta Mater. 2011;59:6588–6593.
[70] Şopu D, Albe K. Influence of grain size and composition, topology and excess free volume on the deformation behavior of Cu–Zr nanoglasses. Beilstein J Nanotechnol. 2015;6:537–545.
[71] Şopu D, Ritter Y, Gleiter H, et al. Deformation behavior of bulk and nanostructured metallic glasses studied via molecular dynamics simulations. Phys Rev B. 2011;83:100202.
[72] Pan J, Wang YX, Guo Q, et al. Extreme rejuvenation and softening in a bulk metallic glass. Nat Commun. 2018;9:560.
[73] Sun Y, Concustell A, Greer AL. Thermomechanical processing of metallic glasses: extending the range of the glassy state. Nat Rev Mater. 2016;1:16039.
[74] Ketov SV, Sun YH, Nachum S, et al. Rejuvenation of metallic glasses by non-affine thermal strain. Nature. 2015;524:200–203.